Journal of Magnetic Resonance 209 (2011) 8–18

Contents lists available at ScienceDirect

Journal of Magnetic Resonance

journal homepage: www.elsevier.com/locate/jmr

Heteronuclear decoupling by multiple rotating frame technique

Haribabu Arthanari [a], Gerhard Wagner [a], Navin Khaneja [b,*]

[a] Department of Biological Chemistry and Molecular Pharamacology, Harvard Medical School, 240 Longwood Avenue, Boston, MA 02115, United States
[b] School of Engineering and Applied Sciences, Harvard University, Cambridge, MA 02138, United States

ARTICLE INFO

Article history:
Received 3 August 2010
Revised 30 November 2010
Available online 6 December 2010

Keywords:
Broadband heteronuclear decoupling
Multiple rotating frame technique
Multiple modulated rf field
Non-resonance conditions (GAP)

ABSTRACT

The paper describes the multiple rotating frame technique for designing modulated rf fields, that perform broadband heteronuclear decoupling in solution NMR spectroscopy. The decoupling method presented here is understood by performing a sequence of coordinate transformations, each of which demodulates a component of the rf field to a static component, that progressively averages the chemical shift and the dipolar interaction. We show that by increasing the number of modulations in the decoupling field, the ratio of dispersion in the chemical shift to the strength of the static component of the rf field is successively reduced in the progressive frames. The known decoupling methods like continuous wave decoupling, TPPM, etc., can be viewed as special cases of this method and their performance improves by adding additional modulations in the decoupling field. The technique is also expected to find use in design of broadband excitation, inversion and mixing sequences and broadband experiments in solid state NMR.

1. Introduction

Heteronuclear decoupling methods have a long history in NMR spectroscopy [1–13,15–27,29,31–33,49–58,61–63] and *in vivo* applications [34–39]. The goal of broadband heteronuclear decoupling sequences is to observe a spin S by irradiating spin I that is coupled to S in order to simplify the spectra and to increase the signal-to-noise ratio. At the same time, the decoupling sequence should introduce only a minimal amount of artifacts, such as decoupling sidebands. Furthermore, in order to avoid undesirable sample heating or damage to the probe, the radio frequency (rf) power of the decoupling sequence should be as small as possible. This is of particular importance in medical imaging or *in vivo* spectroscopy of humans [34–39].

The earliest heteronuclear decoupling methods were based on CW irradiation [10] and noise decoupling [12]. Significantly improved decoupling sequences were found based on composite [8,9,13,15,17–20] or shaped [25–27,29,31,33] inversion pulses in combination with highly compensated cycles and supercycles [8,9,17,40–46]. Theoretical approaches that have been used for the analysis and design of decoupling sequences include average Hamiltonian [16,47,48] and Floquet [32,33] theory.

In this paper, we describe the multiple rotating frame technique for design of heteronuclear decoupling sequences.

In the absence of chemical shifts, the most straightforward way to decouple two heteronuclear spins I and S is to just irradiate with full power on resonance to spin I. However, in the presence of large chemical shifts, one creates an effective field that is not perpendicular to the coupling interaction and therefore part of the coupling interaction parallel to this field is not averaged. We show that it possible to design a multiply-**MOD**ulat**E**d rf field (MODE sequence) for broadband decoupling, whose effect is best understood by performing a sequence of coordinate transformations, *specific to each chemical shift*. Each transformation demodulates a component of the multiply-modulated rf field to a static component. The subsequent transformation is in the rotating frame defined by new static component and the residual chemical shift. Each transformation averages part of the coupling and reduces the ratio of chemical shift interaction to static rf field, progressively making the effective field perpendicular to the coupling interaction. We show that by increasing the number of modulations in the decoupling field, we can significantly improve the decoupling. Methods to make this method robust to rf inhomogeneity are discussed.

2. Heteronuclear decoupling

Consider two heteronuclear spins I and S. The Hamiltonian of the spin system takes the form

$$\mathcal{H}_0 = \omega_I I_z + 2\pi J I_z S_z + \omega_S S_z, \tag{1}$$

where ω_I and ω_S are the chemical shifts of spin I and S. Assuming spin S is being observed, we can without loss of generality take the chemical shift of the spin S to be zero and denoting $\omega_I = \omega$, consider the natural Hamiltonian

* Corresponding author.
E-mail address: navin@hrl.harvard.edu (N. Khaneja).

1090-7807/$ - see front matter © 2010 Elsevier Inc. All rights reserved.
doi:10.1016/j.jmr.2010.11.020

$$\mathscr{H}_0 = \underbrace{\omega I_z}_{H_{cs}} + \underbrace{2\pi J I_z S_z}_{H_c}, \tag{2}$$

where $\omega \in [-c_0, c_0]$. Now, consider the rf Hamiltonian

$$H_0' = w_0 I_x + (w_1 \sin \upsilon_1 t + w_2 \cos \upsilon_1 t \sin \upsilon_2 t + \cdots) I_y. \tag{3}$$

A more general form of the rf Hamiltonian is then

$$H_0' = w_0 I_x + \left(\underbrace{\sum_{k=1}^{N} w_k \prod_{j=1}^{k-1} \cos \upsilon_j t \ \ \sin \upsilon_k t}_{A_0(t)} \right) I_y, \tag{4}$$

where $\upsilon_k > \upsilon_{k+1}$. We adopt the notation $\bar{w}_k = 2^{-k} w_k$, and rewrite the total Hamiltonian $H_0 = \mathscr{H}_0 + H_0'$ as

$$H_0 = \tilde{\omega} I_{z_1(\omega)} + A_0(t) I_y + 2\pi J I_z S_z, \tag{5}$$

where $z_1(\omega)$ is the unit vector along the direction $\omega \hat{z} + w_0 \hat{x}$ and define $\theta_1(\omega) = \tan^{-1}\left(\frac{w_0}{\omega}\right)$, the spread of frequencies $\tilde{\omega} \in \left[w_0, \sqrt{w_0^2 + c_0^2}\right]$. Note, $z_1(\omega)$ is different for each ω. Now, by choosing υ_1 in the first transformation as exactly the center of this spread and transforming into a frame rotating around $I_{z_1(\omega)}$, with frequency υ_1, we get the Hamiltonian

$$H_1 = \underbrace{(\tilde{\omega} - \upsilon_1)}_{f_1(\omega)} I_{z_1(\omega)} + 2\pi J \cos\theta_1(\omega) I_{z_1(\omega)} S_z + \underbrace{\bar{w}_1 I_{x_1} + A_1(t) I_y}_{H_1'} + H_1''(t) + H_1'''(t), \tag{6}$$

where H_1' is the demodulated part of the rf Hamiltonian H_0', in the interaction frame of $I_{z_1(\omega)}$. The form of H_1' resembles H_0'. $H_1''(t)$ and $H_1'''(t)$ are the fast oscillating parts of the rf and coupling Hamiltonian that we ideally want to average out and we neglect these terms for now. $H_1'''(t)$ is simply the part of the coupling perpendicular to the effective field direction $I_{z_1(\omega)}$, that oscillates with frequency υ_1. The new frequency $f_1(\omega) \in [-c_1, c_1]$, where $c_1 < c_0$. A_1, H_1'' and H_1''' are written in their general form below. The system obtained after first coordinate transformation has the desired feature that the ratio of chemical shift spread to static component of the rf field, $\alpha_1 = \frac{c_1}{\bar{w}_1}$ is reduced over $\alpha_0 = \frac{c_0}{w_0}$ for the original system. For example, if $c_0 = w_0$, and $w_1 = w_0$, then $\frac{c_1}{\bar{w}_1} = \sqrt{2} - 1$.

We can now iterate the above construction. We go into successive rotating frames around axis $I_{z_k(\omega)}$ with frequency υ_k. Unit vectors $(x_k(\omega), y_k(\omega), z_k(\omega))$ define the kth frame, where we suppress the argument ω subsequently. $f_k(\omega)$ is the chemical shift in the kth rotating frame, starting with ω in H_0. c_k represents the limit of the chemical shifts in the kth coordinate frame and $\bar{w}_k = 2^{-k} w_k$ is the strength of the rf field along the direction x_k.

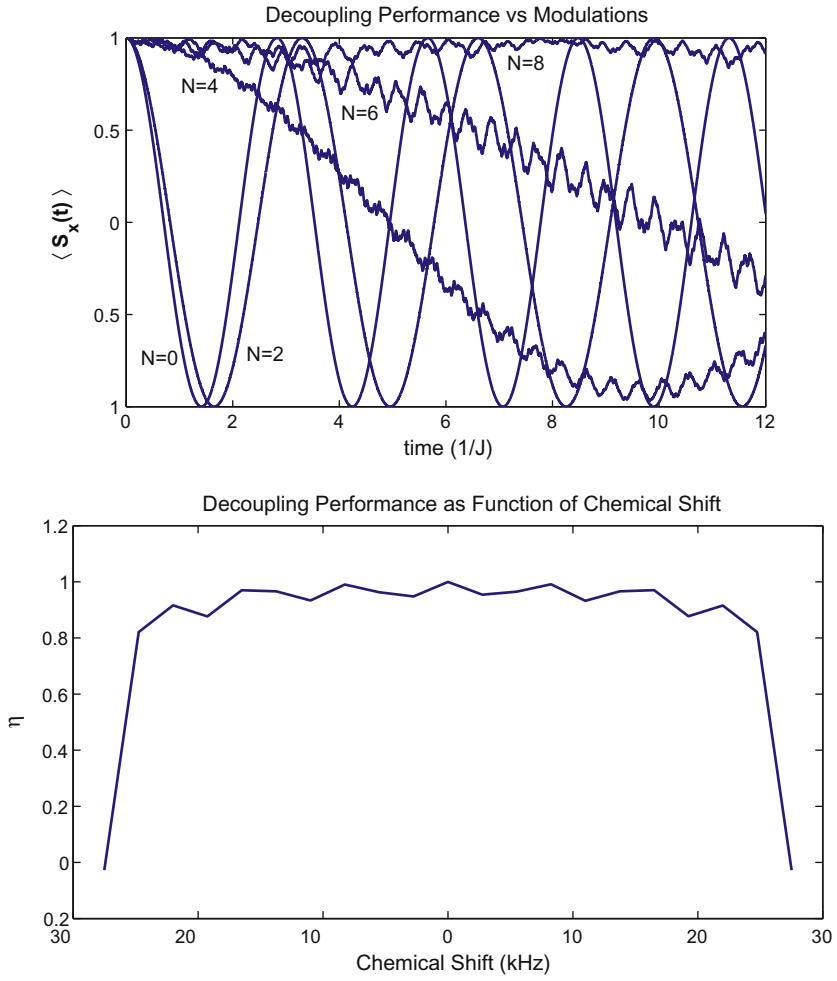

Fig. 1. The top figure shows how the coherence $S_x(t)$ evolves as a function of time in units of J^{-1} as N the number of modulations in the rf field keeping A_{eff} constant. The simulations correspond to $J = 140$ Hz, $A_{eff} = 6.27$ kHz and $\frac{c_0}{2\pi} = 27.5$ kHz corresponding to $\frac{c_0}{2\pi A_{eff}} = 4.39$ and the chemical shift value $\frac{\omega_0}{2\pi A_{eff}} = 1$. The bottom figure shows the decoupling efficiency $\eta = \frac{1}{T}\int_0^T \langle S_x(t)\rangle dt$, as function of ω_0. Here $T = \frac{12}{J} = 85.7$ ms.

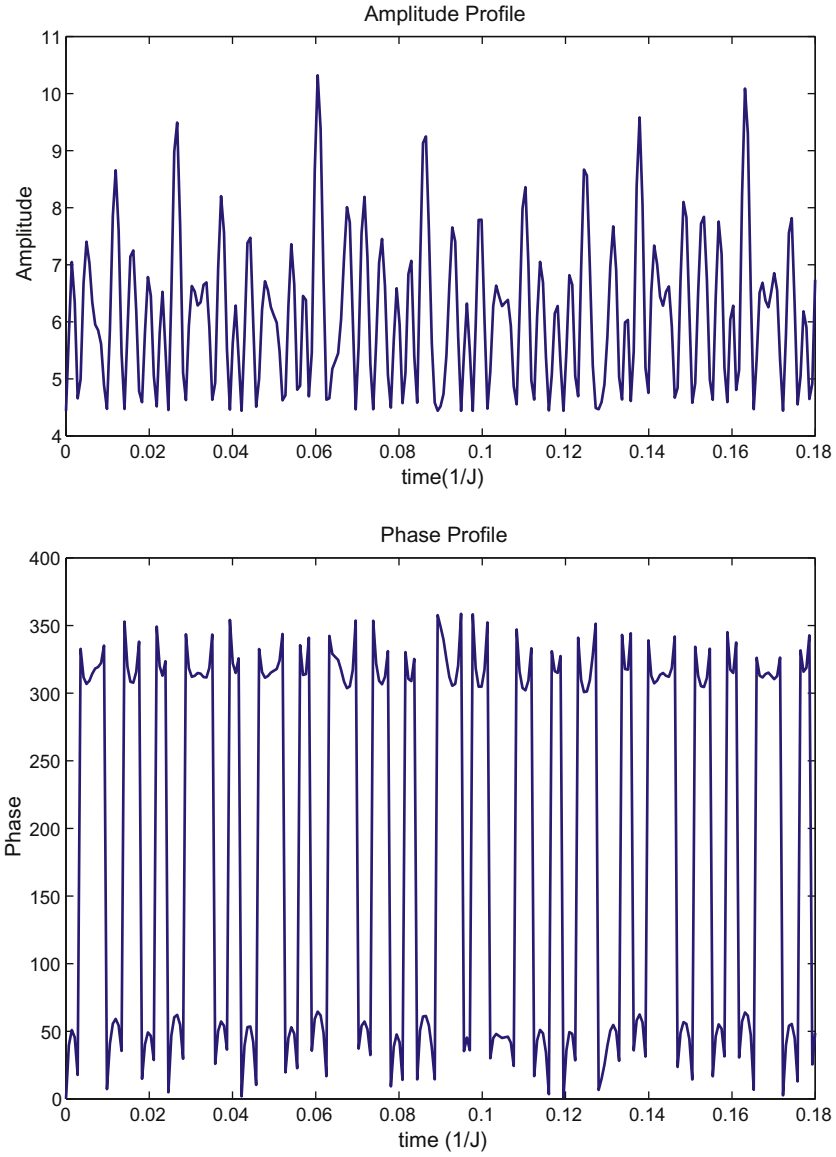

Fig. 2. The top figure shows the amplitude (in kHz) of the rf field as a function of time in units of J^{-1}, corresponding to $N = 8$ modulations, with $\frac{w_0}{2\pi} = 4.44$ kHz. This corresponds to $A_{eff} = 6.27$ kHz. The bottom panel shows the phase (in degrees) as function of time. For $J = 140$ Hz, the time axis corresponds to $\frac{1}{J} = 7.1$ ms.

$$H_k = f_k(\omega) I_{z_{k(\omega)}} + \frac{w_k}{2^k} I_{x_k} + 2\pi J_k I_{z_k} S_z + A_k(t) I_y + H_k''(t) + H_k'''(t), \tag{7}$$

$$A_k(t) = \frac{1}{2^k}\left\{ \sum_{m=k+1}^{n} w_m \prod_{i=k+1}^{m-1} \cos(\upsilon_i t)\sin(\upsilon_m t) \right\} I_y,\ A_n(t) = 0, \tag{8}$$

$$H_k''(t) = \exp(i2\upsilon_k I_{z_k} t)\left(-\frac{w_k}{2^k} I_{x_k} + A_k(t) I_y \right) \exp(-i2\upsilon_k I_{z_k} t), \tag{9}$$

$$H_k'''(t) = J_k^{\perp} \exp(i\upsilon_k I_{z_k} t) I_{x_k} S_z \exp(-i\upsilon_k I_{z_k} t), \tag{10}$$

$$c_{k+1} = \frac{\sqrt{c_k^2 + \bar{w}_k^2} - \bar{w}_k}{2};\ \upsilon_{k+1} = \frac{\sqrt{c_k^2 + \bar{w}_k^2} + \bar{w}_k}{2};\ \tan\theta_k(\omega) = \frac{\bar{w}_k}{f_k(\omega)}, \tag{11}$$

$$J_k = \prod_{j=1}^{k} \cos\theta_j(\omega) J, \tag{12}$$

$$J_k^{\perp} = -\prod_{j=1}^{k-1} \cos\theta_j(\omega)\sin\theta_k(\omega) J. \tag{13}$$

As discussed in the next section the iterated relations on c_k insures that the ratio $\alpha_k = \frac{c_k}{w_k}$ is decreasing and $\theta_k \to \frac{\pi}{2}$. This ensures that $J_k \to 0$.

3. Scaling

To fix ideas, we choose $w_k = w_0$, i.e., $\bar{w}_k = 2^{-k} w_0$. From Eq. (11), we have the relation,

$$\alpha_{k+1} = \sqrt{1 + \alpha_k^2} - 1 < \alpha_k. \tag{14}$$

This ensures that α_k is decreasing. We explore two limits, for $\alpha_k \ll 1$, we obtain,

$$\frac{\alpha_{k+1}}{\alpha_k} \sim \frac{\alpha_k}{2}, \tag{15}$$

$\alpha_k \gg 1$, we have

$$\alpha_{k+1} \sim \alpha_k - 1. \tag{16}$$

Since $\alpha_k \to 0$, we have $\theta_k \to \frac{\pi}{2}$. This ensures that $J_k \to 0$.

We evaluate the root mean square amplitude ($A_{eff} = \sqrt{\frac{1}{T}\int_0^T A^2(\tau) d\tau}$) for this rf field as $N \to \infty$

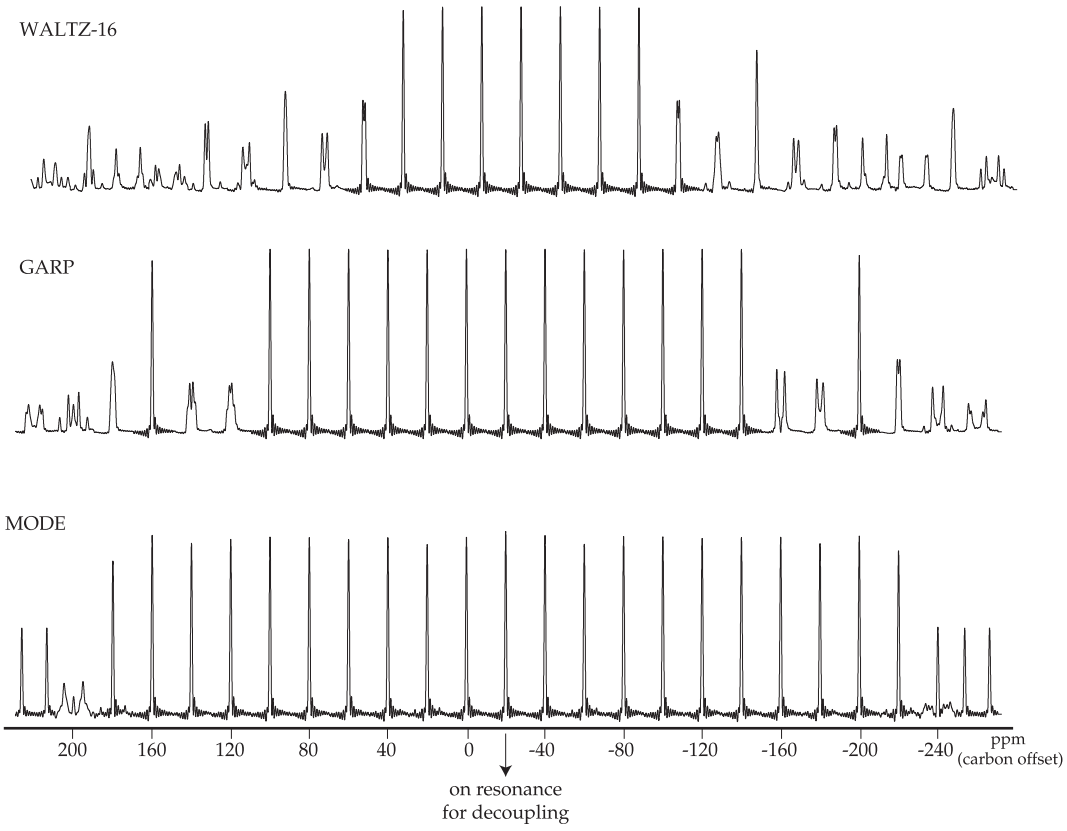

Fig. 3. The above figure show the experimental proton spectra obtained at 500 MHz for a ^{13}C-iodomethane sample, dissolved in D-chloroform (D, 99.8%, Cambridge Isotope Laboratory, Inc.) The top two panels show performance of WALTZ-16 [17] and GARP [19] pulse sequences as function of the offset. The rf field for MODE corresponds to the simulation parameters with $N = 8$ (bottom trace). The A_{eff} for all the decoupling sequence is at 6.27 kHz. The MODE sequence is implemented as small $M = 17{,}136$ flip angle pulses with duration $\Delta = 5$ μs.

$$2\pi A_{eff} = w_0\sqrt{\sum_{k=0}^{N} 2^{-k}} \sim \sqrt{2}w_0. \tag{17}$$

The ratio $\frac{2\upsilon_k}{\bar{w}_k}$ describes how well the oscillating component

$$\bar{w}_k \exp(j2\upsilon_k I_{z_k}) I_{x_k} \exp(-j2\upsilon_k I_{z_k}), \tag{18}$$

is averaged. This ratio

$$\frac{2\upsilon_k}{\bar{w}_k} = 2\left(\sqrt{\alpha_{k-1}^2 + 1} + 1\right) > 4, \tag{19}$$

$$\frac{\upsilon_k}{\upsilon_{k+1}} = \frac{\bar{w}_k}{\bar{w}_{k+1}} \frac{\left(\sqrt{\alpha_k^2 + 1} + 1\right)}{\left(\sqrt{\alpha_{k+1}^2 + 1} + 1\right)} > 2. \tag{20}$$

4. Non-resonant conditions

We now check whether all the oscillating terms captured by Hamiltonians H_k'' and H_k''' that were neglected result in an effective coupling. If this were to happen, in the modulation frame of the rf field and chemical shifts, we will see a net coupling evolution. Therefore, we evaluate the evolution of the couplings in the modulation frame defined by the Hamiltonian $H_m = H_{cs} + H_0'$. The evolution of this frame takes the form

$$U(\omega,t) = \exp(-i\upsilon_1 I_{z_1(\omega)}t)\ldots\exp(-i\upsilon_k I_{z_k(\omega)}t)\ldots\exp(-i\upsilon_N I_{z_N(\omega)}t)\Theta_N(\omega,t),$$

where number of modulations is $N-1$ and

$$\dot{\Theta}_N(\omega) = -i\{f_N(\omega)I_{z(\omega)} + \widetilde{H}(t)\}\Theta_N(\omega), \tag{21}$$

such that $|f_N(\omega)| \ll c_0$. Here, $f_N(\omega)$ represents the chemical shift in the Nth frame. Where

$$\widetilde{H}(t) = \sum_{k=1}^{N-1} V_{k+1}^{\dagger} H_k'' V_{k+1}, \tag{22}$$

where

$$V_k(t) = \exp(-i\upsilon_k I_{z_k}t)\cdots\exp(-i\upsilon_N I_{z_N}t). \tag{23}$$

In this notation,

$$U(\omega,t) = V_1(t)\Theta_N(\omega,t), \tag{24}$$

where

$$\Theta_N(\omega,t) = I - i\int_0^t \widetilde{H}(\tau)d\tau - \int_0^t\int_0^\tau \widetilde{H}(\tau)\widetilde{H}(\sigma)d\tau d\sigma + \cdots. \tag{25}$$

Then in the frame of the Hamiltonian $H_m(t)$, the evolution takes the form

$$I - i2\pi J\int_0^t V_1' I_z S_z V_1 d\tau - \underbrace{2\pi J\int_0^t \left[V_1' I_z S_z V_1, \int_0^\tau \widetilde{H}(\sigma)d\sigma\right]}_{J(\tau)} d\tau + \cdots\cdots \tag{26}$$

where, the first integral is averaged out in the subsequent frames as $\alpha_k \to 0$ and $\upsilon_k > 2\upsilon_{k+1}$ in Eq. (20) prevents generation of static components from the oscillating parts. We evaluate the second integral in the series above. If $J(\tau)$ has any static components this would reflect residual couplings in the system. We use the notation $H_k''(f)$ to denote the discrete set of frequencies present in oscillating Hamiltonian $H_k''(t)$. The discrete frequencies is the set

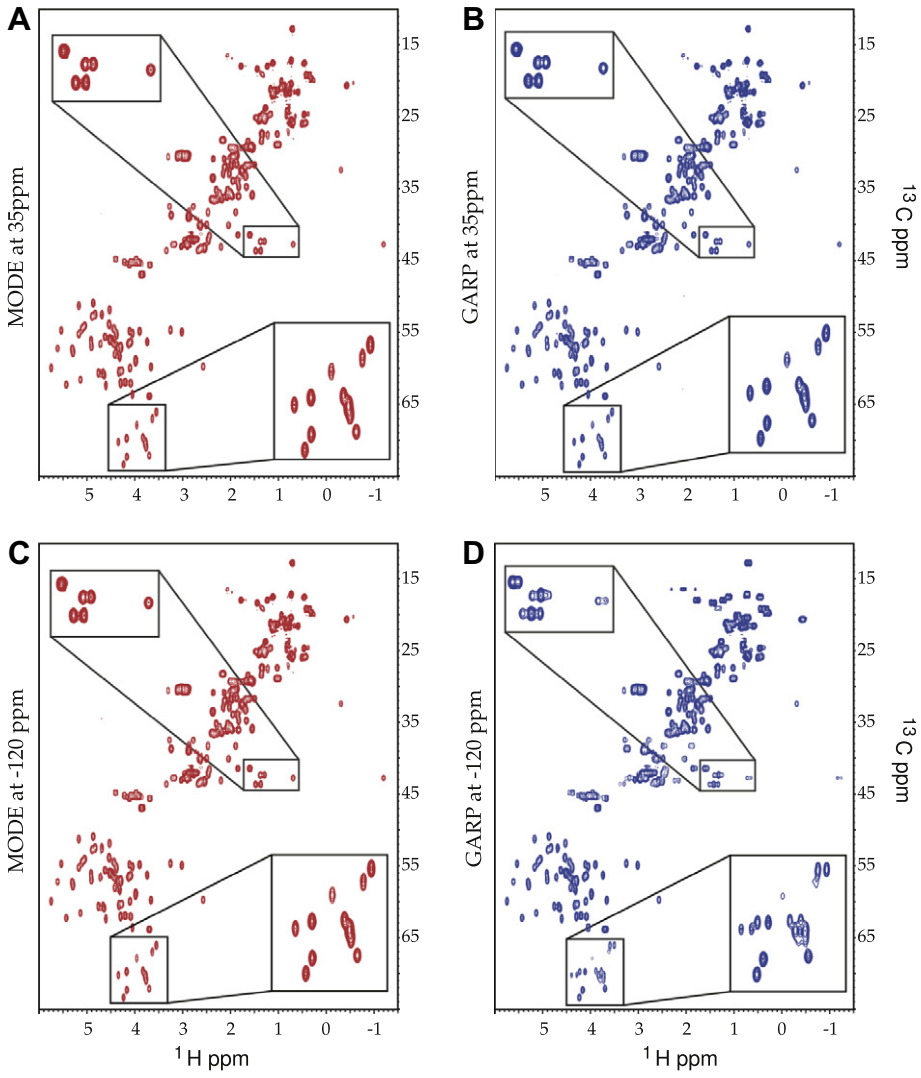

Fig. 4. The above figures show the HSQC spectra on a sample of the protein GB1 obtained at 500 MHz . In the indirect dimension, the proton is decoupled by a refocusing π pulse. In the direct dimension, the carbon is decoupled by application of GARP and MODE decoupling sequences with mean rf amplitude of 6.27 kHz. The MODE sequence used is the same as described earlier in the section. A $^{15}N/^{13}C$ uniformly labeled sample of protein GB1 was prepared to a final concentration of 1 mM in phosphate buffer (20 mM, pH = 6.5) with 150 mM NaCl and 1 mM EDTA. A comparison of decoupling with GARP and MODE with decoupling offsets at 35 ppm and −120 ppm is shown.

$$\{\exp(-i\omega I_\alpha)H_k''\exp(i\omega I_\alpha)\}(f) = \{\omega \pm H_k''(f), \pm H_k''(f)\}, \tag{27}$$

$$(V_{k+1}'H_k''V_{k+1})(f) = a_k\upsilon_k + \sum_{j>k} b_j\upsilon_j, \quad a_k \in \{\pm 2\}, \quad b_j \in \{0, \pm 1, \pm 2\}$$

Similarly, we have

$$V_1'I_zS_zV_1(f) = \sum_{k=1}^{N} c_k\upsilon_k,$$

where $c_k \in \{0, \pm 1\}$. We compute the overlap of the two set of frequencies, we find the smallest value of $|\Delta|$ satisfying

$$\sum_{j=1}^{k} c_j\upsilon_j + a_k\upsilon_k + \sum_{j=k+1}^{N} d_j\upsilon_j = \Delta, \tag{28}$$

where $d_j \in \{0, \pm 1, \pm 2, \pm 3\}$. If $|\Delta| > 0$, we avoid a resonance condition, i.e., the second integral in Eq. (26) has no static components.

4.1. Simulation and experiments

Simulations were carried for a carbon–proton (IS) spin system, with a coupling constant J = 140 Hz in Eq. (1). The carbon chemical shift range was $[-c_0, c_0]$, where $c_0(2\pi)^{-1}$ = 27.5 kHz, which corresponds to a 244 ppm carbon chemical shift range at 900 MHz proton frequency. At 6.25 kHz rf power, the $\frac{\pi}{2}$ pulse corresponds to 40 μs. We choose $w_k = w_0$, and calculate w_0 that corresponds to $A_{eff} \sim 6.25$ kHz. For $N = 8$, this corresponds to $\frac{w_0}{2\pi} = 4.44$ kHz (for $n \geqslant 4, \frac{w_0}{2\pi} \sim \frac{A_{eff}}{\sqrt{2}}$). w_0 may be adjusted if the resulting rms power $\widetilde{A}_{eff}$, is not exactly A_{eff}. For $N = 8$, the parameter $\alpha_N = .1$ and the sequence is broadband over the given bandwidth, see Fig. 1. The resulting A_{eff} = 6.27 kHz. Fig. 2 shows the amplitude and phase profile of the MODE sequence. Fig. 1 shows evolution of initial magnetization $\langle S_x(0)\rangle = 1$ under the MODE sequence for various values of N at $A_{eff} = 6.27 \pm .02$ kHz, for a period of $\sim 12\,J^{-1}$. Fig. 1 also shows the decoupling efficiency as time averaged x-magnetization on spin S [59],

$$\eta = \frac{1}{T}\int_0^T \langle S_x(t)\rangle dt, \tag{29}$$

for various offsets.

The parameters of the MODE sequence for $N = 8$, $w_0 = w_k = 4.44$, $c_0 = 27.5$, $c_1 = 11.7$, $c_2 = 4.85$, $c_3 = 1.93$, $c_4 = .73$, $c_5 = .25$, $c_6 = .07$, $c7 = .016$ and $c_8 = .002$, all in units of 2π kHz. The modulation

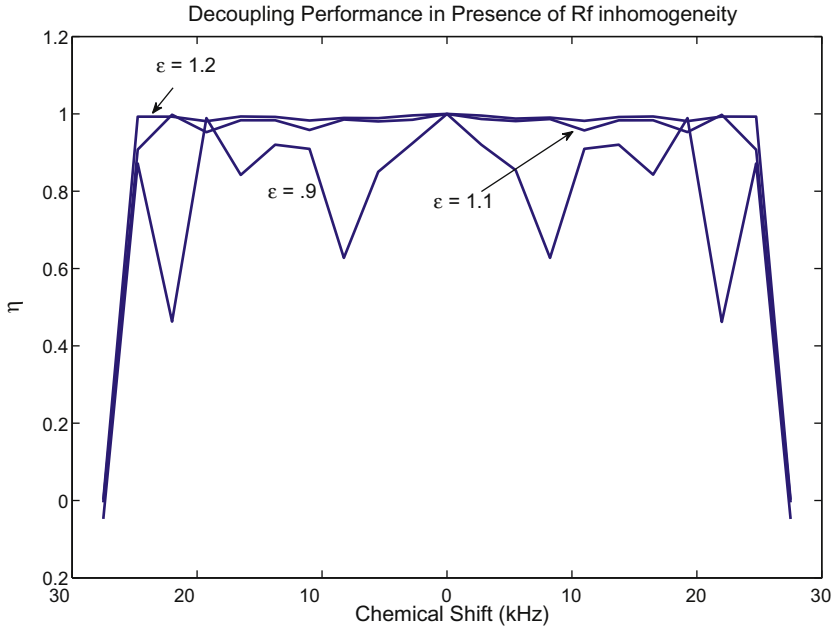

Fig. 5. The above figure shows the decoupling efficiency η, as function of ω_0. Here $T \sim \frac{12}{J} \sim 85.7$ ms for rf inhomogeneity values corresponding to $\epsilon = .9$, $\epsilon = 1.1$ and $\epsilon = 1.2$ with $\delta = -.1$, $\delta = .1$ and $\delta = .2$ respectively. The mode sequence is designed with $N = 8, \frac{c_0}{w_0} = 4.39$ and $c_0 = 27.5$ kHz.

frequencies are $\upsilon_1 = 16.15$, $\upsilon_2 = 7.07$, $\upsilon_3 = 3.04$, $\upsilon_4 = 1.28$, $\upsilon_5 = 0.53$ and $\upsilon_6 = 0.21$, $\upsilon_7 = .085$ and $\upsilon_8 = .0364$ all in units of 2π kHz. The ratio $\frac{c_0}{w_0} = 6.2$, $\frac{c_1}{w_1} = 5.28$, $\frac{c_2}{w_2} = 4.37$, $\frac{c_3}{w_3} = 3.48$, $\frac{c_4}{w_4} = 2.62$, $\frac{c_5}{w_5} = 1.81$, $\frac{c_6}{w_6} = 1.07$, $\frac{c_7}{w_7} = .46$, and $\frac{c_8}{w_8} = .10$. In the last frame, the ratio of chemical shift to effective control is significantly reduced. The smallest frequency in Eq. (28) is .001 Hz, for the combination $(\upsilon_1 - 2\upsilon_2 + \upsilon_3 - 3\upsilon_4 - 2\upsilon_5 - \upsilon_6 + \upsilon_7 - 2\upsilon_8 + 3\upsilon_9)$, where $\upsilon_9 = .0175$, in the units of 2π Hz. See Supplementary material for another design of a MODE sequence with $N = 6$.

The decoupling efficiency of the MODE decoupling sequence was studied experimentally using a ^{13}C-iodomethane sample, dissolved in deuterated-chloroform. The experiments were carried out on a 500 MHz Bruker spectrometer at room temperature. The MODE pulse sequence can be implemented on a spectrometer, as sequence of small flip angle pulses with defined amplitude and phases. The MODE sequence of duration $T = \frac{12}{J} = 85.7$ ms is finely discretized in M steps to capture all its modulations. The discretization used corresponds to $\Delta \sim \frac{.51}{\upsilon_1}$ and $M = 17{,}136$ (a finer discretization may be used), and A_{eff} for this discretized sequence is 6.27 kHz. The closed form formula for the MODE sequence (4) is in terms of the amplitude of the x and y component of the rf-Hamiltonian, which allows the computation of the amplitude $A_k = (2\pi)^{-1}\sqrt{A_0^2(k\Delta) + w_0^2}$ and the phase $\tan\phi_k = \frac{A_0(k\Delta)}{w_0}$, for the kth pulse. The MODE sequence was implemented as a table of amplitude and phases, where the amplitudes are specified as percentage of the peak amplitude.

Proton resonances were observed with carbon decoupling during acquisition. A thousand two hundred points were collected with a dwell-time of 71.4 μs and a total acquisition time of 85.7 ms. Sixteen scans were averaged with a recycle delay of 15 s between them. The carbon resonance of iodomethane occurs at −20.7 ppm. The offset on the carbon channel (decoupling offset) was varied from −240 to 220 ppm to study the effect of the various decoupling sequences.

Fig. 3 shows the experimental spectra obtained on a system of methyl iodide with MODE sequence. The experimental parameters of the system are the same as in simulations. Comparison of conventional decoupling sequences with MODE shows it is more broadband for the same root mean square rf power.

Fig. 4 shows the 2D ^{13}C HSQC spectra of the protein GB1, comparing GARP and MODE decoupling sequences on ^{13}C during direct detection. ^{1}H–^{13}C HSQC experiments were collected with 128 complex points in the indirect (^{13}C) dimension and 1200 points in the

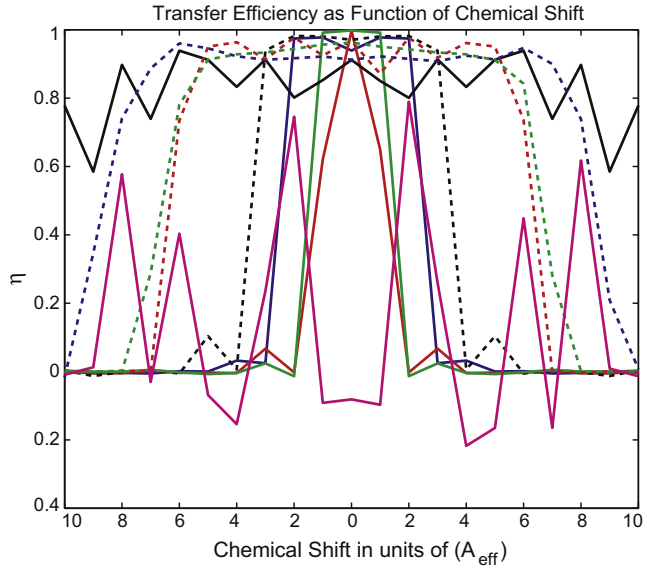

Fig. 6. The above figure shows performance of the state of the art decoupling sequences as a function of the chemical shifts. MODE (black), SUSAN (dashed black) [60], GARP (blue) [19], WALTZ-16 (green) [17], MLEV-16 (red) [14], CHIRP (dashed blue) [30], STUD (dashed red) [26], MPF9 (dashed green) [24], WURST (magenta) [28]. The acquisition time of $72J^{-1}$, which for a coupling of 140 Hz translates to ∼510 ms. The performance parameter η is plotted as a function of chemical shift in units of root mean square amplitude A_{eff}. We use $A_{eff} = 2.25$ kHz such that a total bandwidth of $20A_{eff}$ corresponds to 45 kHz. The various pulse sequences were implemented exactly the way described in their respective references. The coupling and the acquisition time was scaled so that at the scaled rms amplitude of 2.25 kHz, all pulse sequences see a coupling of 140 Hz and acquisition time of ∼510 ms.

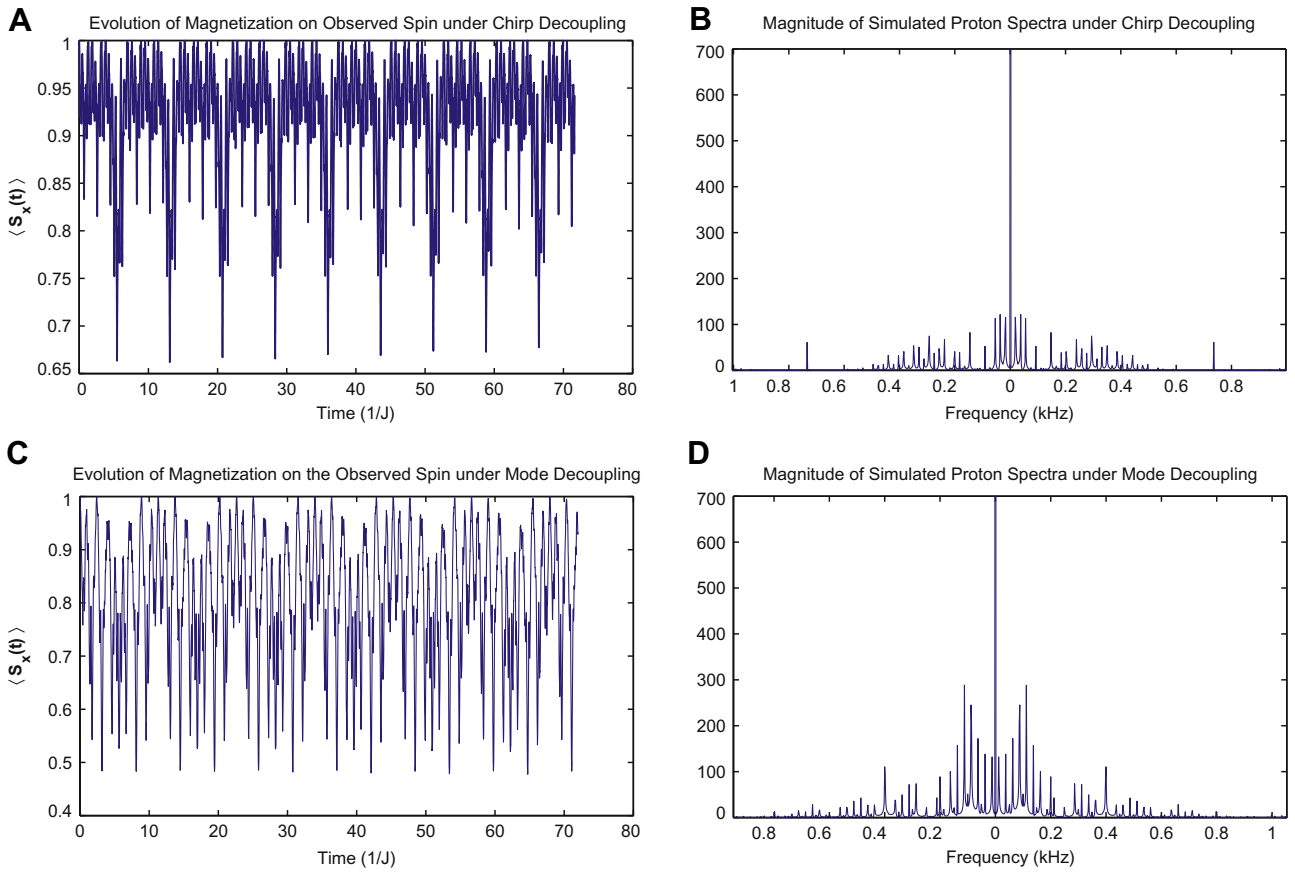

Fig. 7. Comparison of CHIRP (top) and MODE decoupling (bottom). Panel A shows simulation for time evolution of proton magnetization under CHIRP decoupling [30], for a duration of $72J^{-1}$, which for a coupling of 140 Hz, translates to ~510 ms with A_{eff} = 2.25 kHz. Panel C shows the same evolution under MODE decoupling. The parameters of the MODE decoupling sequences are described as above and the CHIRP decoupling sequence is as in [30]. B and D shows the Fourier transform of this time evolution. In both cases we take approx 7200 points, which corresponds to a spectral width of ~14 kHz. The offset for the irradiated ^{13}C is taken to be $4A_{eff}$, i.e. 9 kHz. Limits on vertical axis in B and D are chosen to magnify any modulation sidebands. The magnitude of the primary resonance is outside the scale limits.

direct (^{1}H) dimension with eight scans for every indirect point with a recycle delay of 3 s. The carrier was centered at 4.7 ppm on the proton channel and 35 ppm on the carbon channel. The carrier on the carbon channel is shifted before acquisition/decoupling to study the broadband performance of decoupling sequences. With the MODE decoupling we observe H-alpha protons that are attached to the down field carbon C-alpha (50–60 ppm) to be decoupled even when the carbon carrier was shifted to −120 ppm. In case of the GARP decoupling, we observe minor imperfections in decoupling (highlighted and zoomed in boxed regions) under similar conditions. These experiments also show that MODE sequences can be readily incorporated in standard NMR experiments.

Fig. 5 shows simulations of the performance of the MODE decoupling sequence as function of rf inhomogeneity, which is captured by the parameter $\epsilon = (1 + \delta)$, such that the actual amplitude of the rf field is ϵA where A is the nominal amplitude.

In the absence of inhomogeneity, for all $\omega \in [-c_0,\ c_0]$, $f_k(\omega) \leqslant f_k(c_0)$ and the ratio $\frac{c_k}{\bar{w}_k}$ is constantly decreasing. In the presence of rf inhomogeneity, for our simulation with $\delta = .1$ and $\delta = .2$, it is observed that $\frac{f_k(c_0)}{\bar{w}_k}$ begins to increase. For $\delta = -.1$, we observe that $f_k(\omega) \not\leqslant f_k(c_0)$. The performance of the MODE sequence in the presence of rf inhomogeneity for $\delta > 0$ is comparable to the ideal case. For $\delta = -.1$, offset frequencies are affected by rf inhomogeneity. The angle $\prod_k \cos(\theta_k)$ in (12) (measuring residual coupling) is largest for the offset at ±8.25 kHz which is close to resonance rather than at the extreme. This may be attributed to $f_k(\omega) \not\leqslant f_k(c_0)$. These simulations suggest that operating the MODE sequence slightly above the nominal value can alleviate the performance of MODE for rf values below nominal.

Alternatively, in the presence of rf inhomogeneity, we can redefine our iterative procedure for computing the modulation frequencies υ_k. In presence of inhomogeneity, the spread of effective shifts after the first frame transformation is from $\left[(1-\delta)w_0, \sqrt{(1+\delta)^2 w_0^2 + c_0^2}\right]$, the left limit corresponds to zero offset and smallest rf amplitude. The right limit corresponds to largest rf amplitude and chemical shift. We choose υ_1 as center of this spread. Following this we obtain that

$$\upsilon_{k+1} = \frac{\sqrt{c_k^2 + \bar{w}_k^2(1+\delta)^2} + \bar{w}_k(1-\delta)}{2};$$
$$c_{k+1} = \frac{\sqrt{c_k^2 + \bar{w}_k^2(1+\delta)^2} - \bar{w}_k(1-\delta)}{2}. \tag{30}$$

This gives

$$\alpha_{k+1} = \sqrt{\alpha_k^2 + (1+\delta)^2} - (1-\delta). \tag{31}$$

Note

$$\sqrt{\alpha_k^2 + (1+\delta)^2} - (1-\delta) \leqslant \alpha_k, \tag{32}$$

with equality when

$$\alpha_k = \alpha_p = \frac{2\delta}{1-\delta}.$$

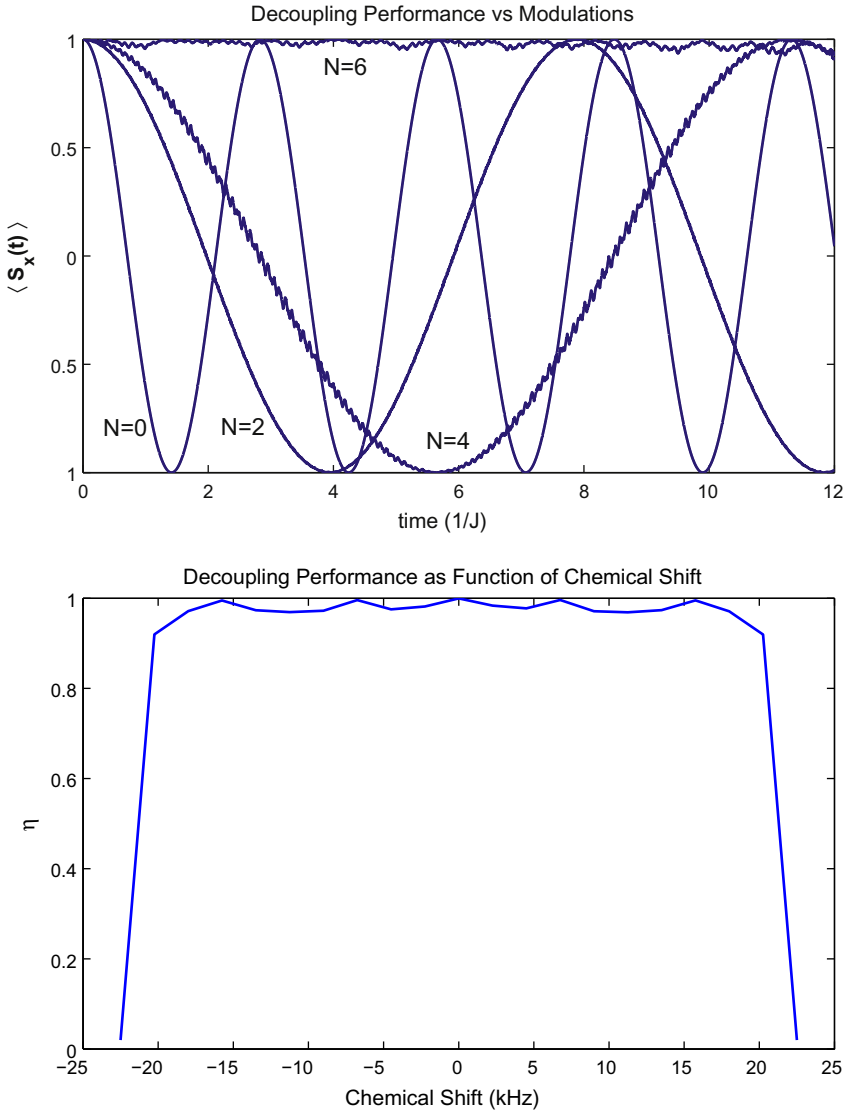

Fig. 8. The top figure shows how the coherence $S_x(t)$ evolves as a function of time in units of J^{-1} as N the number of modulations in the rf field keeping A_{eff} constant. The simulations correspond to $J = 140$ Hz, $A_{eff} = 6.25$ kHz and $\frac{c_0}{2\pi} = 22.5$ kHz corresponding to $\frac{c_0}{2\pi A_{eff}} = 3.6$ and the chemical shift value $\frac{\omega_0}{2\pi A_{eff}} = 1$. The bottom figure shows the decoupling efficiency $\eta = \frac{1}{T}\int_0^T \langle S_x(t)\rangle dt$, as function of ω_0. Here $T = \frac{12}{J} = 85.7$ ms.

The α_k values decrease until they reach α_p. For $\delta = .1$, we have $\alpha_p \sim .22$, which is good enough as the ratio of chemical shift to rf strength is small. More generally, relaxing the constraint, $w_{k+1} = w_k$, we can move this fixed point close to zero.

5. Discussion and conclusion

The Fig. 6 simulates performance of the state of the art decoupling pulse sequences for an acquisition time of $72\,J^{-1}$, which for a coupling of 140 Hz translates to 510 ms. The performance parameter η is plotted as a function of chemical shift in units of rms amplitude A_{eff}. We use $A_{eff} = 2.25$ kHz, such that a total bandwidth of 20 A_{eff}, corresponds to 45 kHz, the full 200 ppm carbon spectra on a 900 MHz spectrometer. The various pulse sequences were implemented exactly the way described in their respective references. The coupling and the acquisition time was scaled so that at the scaled rms amplitude of 2.25 kHz, all pulse sequences see a coupling of 140 Hz and acquisition time of ~510 ms. The parameters for the MODE pulse sequence are $N = 9$, $w_0 = 0.2250$, $w_1 = 0.4460$, $w_2 = 0.8762$, $w_3 = 1.6916$, $w_4 = 3.1565$, $w_5 = 5.5235$, $w_6 = 8.6296$, $w_7 = 11.3585$, $w_8 = 12.4943$, $w_9 = 6.3103$, all in units of 2π kHz. This corresponds to a rms amplitude of $A_{eff} = 2.25$ kHz. The chemical shifts in the various frames is $c_0 = 25.0150$, $c_1 = 12.3955$, $c_2 = 6.0873$, $c_3 = 2.9361$, $c_4 = 1.3661$, $c_5 = 0.5915$, $c_6 = .2218$, $c_7 = .0624$, $c_8 = .0099$, $c_9 = .0005$, all in units of 2π kHz. The ratio of the chemical shifts to static rf control in each frame is $\frac{c_0}{w_0} = 111.1779$, $\frac{c_0}{w_0} = 55.5867$, $\frac{c_0}{w_0} = 27.7889$, $\frac{c_0}{w_0} = 13.8854$, $\frac{c_0}{w_0} = 6.9248$, $\frac{c_0}{w_0} = 3.4268$, $\frac{c_0}{w_0} = 1.6448$, $\frac{c_0}{w_0} = 0.7027$, $\frac{c_0}{w_0} = 0.2020$, $\frac{c_0}{w_0} = 0.0400$. In the last frame, the ratio of chemical shift to effective control is significantly reduced. The various modulation frequencies are $\upsilon_1 = 12.6205$, $\upsilon_2 = 6.3103$, $\upsilon_3 = 3.1551$, $\upsilon_4 = 1.5776$, $\upsilon_5 = 0.7888$, $\upsilon_6 = 0.3944$, $\upsilon_7 = .1972$, $\upsilon_8 = 0.0986$, $\upsilon_9 = .0493$ in units of 2π kHz. Note, since we are using low rf power, the starting value α_0 is large. Eq. (16) entails that in this limit $\alpha_{k+1} \sim \alpha_k - 1$. This will require large number of modulations N to reduce α_N below a desired threshold. To achieve a faster decrease in the value of α_k, we start with the an acceptable value of α_N in the final frame which is chosen to be $\alpha_N = .04$ and $\upsilon_N = 4\bar{w}_N$. We solve the forward equations

$$c_{k+1} = \frac{\sqrt{c_k^2 + \bar{w}_k^2} - \bar{w}_k}{2}; \quad \upsilon_{k+1} = \frac{\sqrt{c_k^2 + \bar{w}_k^2} + \bar{w}_k}{2}. \tag{33}$$

backwards, by choosing $\upsilon_k = 2\upsilon_{k+1}$, and

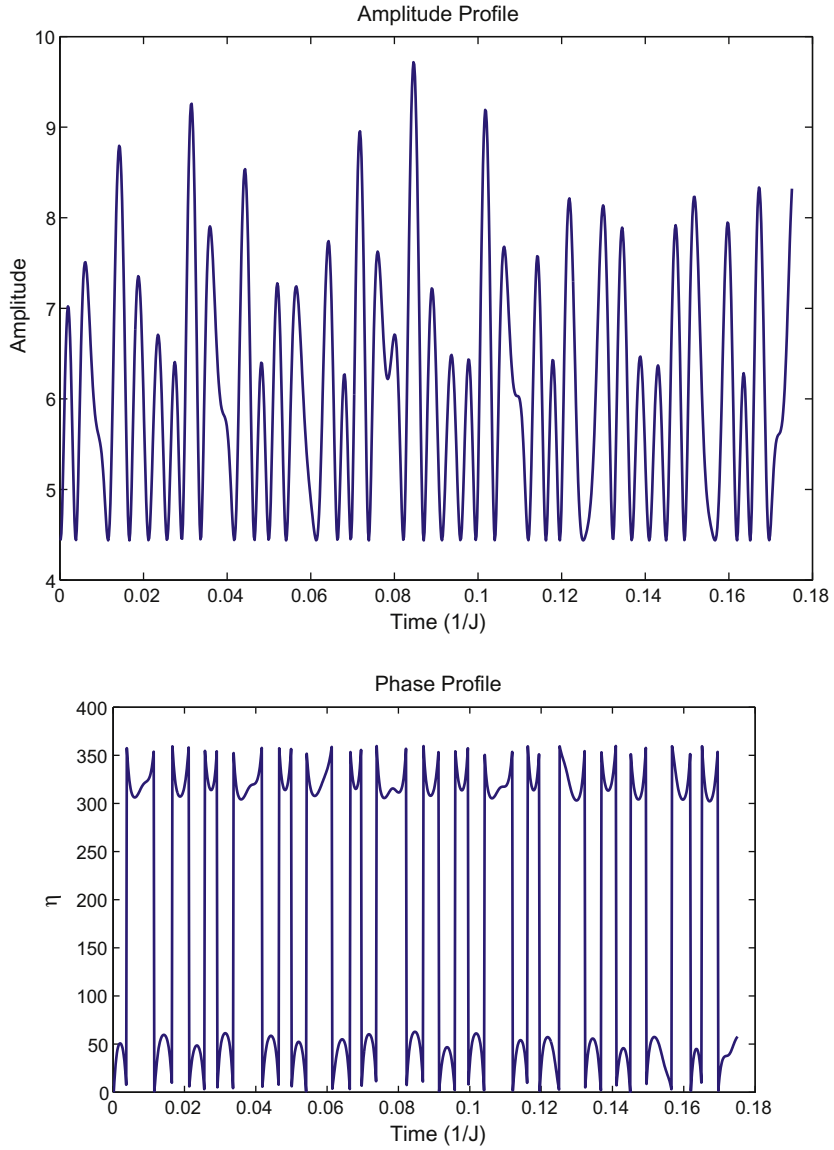

Fig. 9. The top figure shows the amplitude (in kHz) of the rf field as a function of time in units of J^{-1}, corresponding to $N = 6$ modulations, with $\frac{w_0}{2\pi} = 4.44$ kHz. This corresponds to $A_{eff} = 6.25$ kHz. The bottom panel shows the phase (in degrees) as function of time. For $J = 140$ Hz, the time axis corresponds to $\frac{1}{J} = 7.1$ ms.

$$c_k = 2\sqrt{c_{k+1}\upsilon_{k+1}}; \quad \bar{w}_k = \upsilon_{k+1} - c_{k+1}. \tag{34}$$

We stop, when $\alpha_k > \alpha_0$. All the parameters can now be renormalized to achieve desired A_{eff}. It can be shown that growth of α_k, working backwards as in Eq. (34) is exponential, giving relatively fewer number of modulations for which α_0 is the desired value at low powers.

Adiabatic sequences are relatively broadband at low powers as seen in Fig. 6. In Fig. 7, MODE decoupling sequence is compared with an adiabatic decoupling sequence like CHIRP, in terms of the modulation sidebands.

In this paper, we introduced the multiple rotating field technique as a means to design broadband heteronuclear decoupling sequences in solution NMR. It is important to point out that the MODE sequences for the case when $N = 1$, simply reduce to the presence of a second oscillating field, as in [10] and the well known TPPM decoupling pulse sequence [1]. Also see [2–7]. The main contribution of this paper lies in realizing the importance of the ratio α_k and showing that by adding extra modulations in the rf field and successively transforming into rotating frames, we can significantly reduce the ratio α_k and improve the decoupling performance. The technique is also expected to find use in design of broadband excitation, inversion and mixing sequences, and design of broadband experiments in solid state NMR, where spread of chemical shifts can simply be removed by transforming into a suitable K frame.

The parameters of the MODE sequence for $N = 6$, are $J = 140$ Hz, $A_{eff} = 6.25$ kHz, $w_0 = w_k = 4.44$, $c_0 = 22.5$, $c_1 = 9.25$, $c_2 = 3.65$, $c_3 = 1.35$, $c_4 = .45$, $c_5 = .13$, $c_6 = .02$, all in units of 2π kHz. The modulation frequencies are $\upsilon_1 = 13.68$, $\upsilon_2 = 5.86$, $\upsilon_3 = 2.46$, $\upsilon_4 = 1.01$, $\upsilon_5 = 0.40$ and $\upsilon_6 = 0.1633$, all in units of 2π kHz. The ratio $\frac{c_0}{w_0} = 5.07$, $\frac{c_1}{w_1} = 4.17$, $\frac{c_2}{w_2} = 3.29$, $\frac{c_3}{w_3} = 2.44$, $\frac{c_4}{w_4} = 1.63$, $\frac{c_5}{w_5} = .914$, $\frac{c_6}{w_6} = .355$. The total time $T = 85.7$ ms. The smallest frequency $|\Delta|$ in Eq. (28) is .34 Hz, for the combination $(\upsilon_1 - 3\upsilon_2 + 3\upsilon_4 + 3\upsilon_5 - 2\upsilon_6)$. See Figs. 8–10 for simulation and experimental results with MODE sequence with $N = 6$.

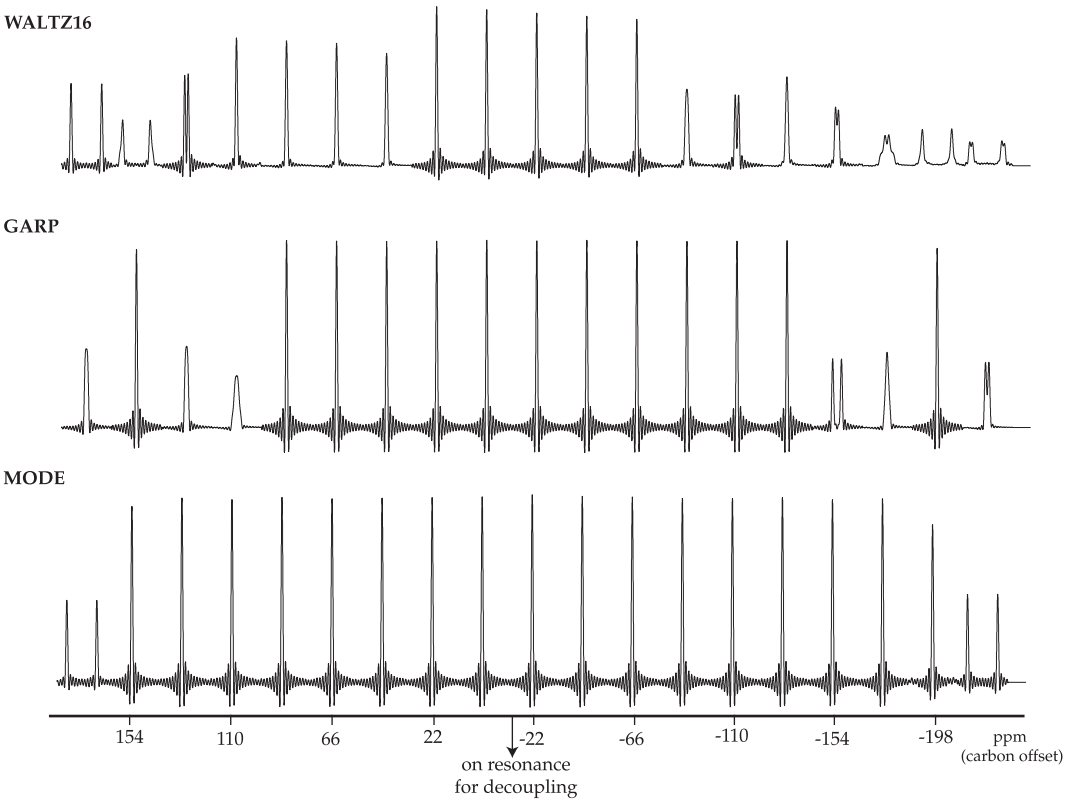

Fig. 10. The above figure show the experimental proton spectra obtained at 500 MHz for a ^{13}C-iodomethane sample, dissolved in D-chloroform (D, 99.8%, Cambridge Isotope Laboratory, Inc.). 16 scans were averaged. The top two panels show performance of WALTZ-16 [17] and GARP [19] pulse sequences as function of the offset. The rf field corresponds to the simulation parameters with $N = 6$. The A_{eff} for the sequences is at ~6.25 kHz (bottom trace). The MODE sequence is implemented as small $M = 68544$ flip angle pulses with duration $\Delta = 1.3$ μs corresponding to $\Delta = \frac{1}{9\nu_1}$.

Acknowledgments

Authors would like to thank Prof. Steffen J. Glaser for helpful discussions on the subject and pointing out a complete set of Ref. [59]. N. K. will like to acknowledge Sinbae Kim for fruitful discussions on Eq. (34), [64] and Paul Coote for discussion on Eq. (30–32), as part of an independent study course. N.K. will like to acknowledge NSF-0724057, ONR 38A-1077404 and AFOSR FA9550-05-1-0443 for supporting this work. G.W. would like to thank P01-GM047467 for supporting this work.

References

[1] A.E. Benett, C.M. Rienstra, M. Auger, K.V. Lakshmi, R.G. Griffin, J. Chem. Phys. 103 (1995) 6951.
[2] B.M. Fung, A.K. Khitrin, K. Ermolaev, J. Magn. Reson. 142 (2000) 97.
[3] Z.H. Gan, R.R. Ernst, Solid State NMR 8 (1997) 153.
[4] M. Eden, M.H. Levitt, J. Chem. Phys. 111 (1999) 1511.
[5] Y. Yu, M.M. Fung, J. Magn. Reson. 130 (1998) 317.
[6] K. Takegoshi, J. Mizokami, T. Terao, Chem. Phys. Lett. 341 (2001) 540.
[7] A. Detken, E. Hardy, M. Ernst, B. Meier, Chem. Phys. Lett. 356 (2002) 298–304.
[8] M.H. Levitt, R. Freeman, T.A. Frenkiel, Broadband decoupling in high-resolution NMR spectroscopy, Adv. Magn. Reson. 11 (1983) 47–110.
[9] A.J. Shaka, J. Keeler, Broadband spin decoupling in isotropic liquids, Prog. NMR Spectrosc. 19 (1987) 47–129.
[10] W.A. Anderson, R. Freeman, Influence of a second radiofrequency field on high-resolution nuclear magnetic resonance spectra, J. Chem. Phys. 37 (1962) 85–103.
[11] W.A. Anderson, F.A. Nelson, Removal of residual splitting in nuclear magnetic double resonance, J. Chem. Phys. 39 (1963) 183–189.
[12] R.R. Ernst, Nuclear magnetic double resonance with an incoherent radio-frequency field, J. Chem. Phys. 45 (1966) 3845–3861.
[13] R. Freeman, S.P. Kempsell, M.H. Levitt, Broadband decoupling and scaling of heteronuclear spin–spin interactions in high-resolution NMR, J. Magn. Reson. 35 (1979) 447–450.
[14] M.H. Levitt, R. Freeman, J. Magn. Reson. 43 (1981) 502.
[15] M.H. Levitt, R. Freeman, T. Frenkiel, Broadband heteronuclear decoupling, J. Magn. Reson. 47 (1982) 328–330.
[16] J.S. Waugh, Theory of broadband spin decoupling, J. Magn. Reson. 50 (1982) 30–49.
[17] A.J. Shaka, J. Keeler, T. Frenkiel, R. Freeman, An improved sequence for broadband decoupling: WALTZ-16, J. Magn. Reson. 52 (1983) 335–338.
[18] A.J. Shaka, J. Keeler, R. Freeman, Evaluation of a new broadband decoupling sequence: WALTZ-16, J. Magn. Reson. 53 (1983) 313–340.
[19] A.J. Shaka, P.B. Barker, R. Freeman, Computer-optimized decoupling scheme for wideband applications and low-level operation, J. Magn. Reson. 64 (1985) 547–552.
[20] T. Fujiwara, K. Nagayama, Composite inversion pulses with frequency switching and their application to broadband decoupling, J. Magn. Reson. 77 (1988) 53–63.
[21] E.R.P. Zuiderweg, S.W. Fesik, Band-selective heteronuclear decoupling using shaped pulses as an aid in measuring long-range heteronuclear coupling constants, J. Magn. Reson. 93 (1991) 653–658.
[22] U. Eggenberger, P. Schmidt, M. Sattler, S.J. Glaser, C. Griesinger, Frequency-selective decoupling with recursively expanded soft pulses in multinuclear NMR, J. Magn. Reson. 100 (1992) 604–610.
[23] M.A. McCoy, L. Mueller, Selective decoupling, J. Magn. Reson. A 101 (1993) 122–130.
[24] T. Fujiwara, T. Anai, N. Kurihara, K. Nagayama, Frequency-switched composite pulses for decoupling carbon-13 spins over ultrabroad bandwidths, J. Magn. Reson. A 104 (1993) 103–105.
[25] Z. Starcuk Jr., K. Bartusek, Z. Starcuk, Heteronuclear broadband spin-flip decoupling with adiabatic pulses, J. Magn. Reson. A. 107 (1994) 24–31.
[26] M.R. Bendall, Broadband and narrowband spin decoupling using adiabatic spin flips, J. Magn. Reson. A 112 (1995) 26–129.
[27] T.E. Skinner, M.R. Bendall, Peak power and efficiency in hyperbolic secant decoupling, J. Magn. Reson. A 123 (1995) 111–115.
[28] E. Kupce, R. Freeman, Adiabatic pulses for wideband inversion and broadband decoupling, J. Magn. Reson. A 115 (1995) 273–276.
[29] E. Kupce, R. Freeman, Optimized adiabatic pulses for wideband spin inversion, J. Magn. Reson. A 118 (1996) 299–303.
[30] R. Fu, G. Bodenhausen, Broadband decoupling in NMR with frequency-modulated 'chirp' pulses, Chem. Phys. Lett. 245 (1995) 415–420.
[31] R. Fu, G. Bodenhausen, Evaluation of adiabatic frequency-modulated schemes for broadband decoupling in isotropic liquids, J. Magn. Reson. A 119 (1996) 129–133.
[32] H. Geen, Theoretical design of amplitude-modulated pulses for spin decoupling in nuclear magnetic resonance, J. Phys. B 29 (1996) 1699–1710.
[33] H. Geen, J.-M. Böhlen, Amplitude-modulated decoupling pulses in liquid state NMR, J. Magn. Reson. 125 (1997) 376–382.

[34] P.A. Bottomley, C.J. Hardy, P.B. Roemer, O.M. Mueller, Proton-decoupled, overhauser-enhanced, spatially localized carbon-13 spectroscopy in humans, Magn. Reson. Med. 12 (1989) 348–363.
[35] D.M. Freeman, R. Hurd, Decoupling: theory and practice II. State of the art in vivo applications of decoupling, NMR Biomed. 10 (1997) 381–393.
[36] P.B. Barker, X. Golay, D. Artemor, R. Ouwerkerk, M.A. Smith, A.J. Shaka, Broadband proton decoupling for in vivo brain spectroscopy in humans, Magn. Reson. Med. 45 (2001) 226–232.
[37] R.A. de Graaf, Theoretical and experimental evaluation of broadband decoupling techniques for in vivo nuclear magnetic resonance spectroscopy, Magn. Reson. Med. 53 (2005) 1297–1306.
[38] S. Li, J. Yang, J. Shen, Novel strategy for cerebral ^{13}C MRS using very low rf power for proton decoupling, Magn. Reson. Med. 57 (2007) 265–271.
[39] A.P. Chen, J. Tropp, R.E. Hurd, M. Van Criekinge, L.G. Carvajal, D. Xu, J. Kurhanewicz, D.B. Vigneron, *In vivo* hyperpolarized ^{13}C MR spectroscopy imaging with ^{1}H decoupling, J. Magn. Reson. 197 (2009) 100–106.
[40] M.H. Levitt, R. Freeman, T. Frenkiel, Supercycles for broadband heteronuclear decoupling, J. Magn. Reson. 50 (1982) 157–160.
[41] M.H. Levitt, R.R. Ernst, Composite pulses constructed by a recursive expansion procedure, J. Magn. Reson. 55 (1983) 247–254.
[42] R. Tycko, A. Pines, J. Guckenheimer, Fixed point theory of iterative excitation schemes in NMR, J. Chem. Phys. 83 (1985) 2775–2802.
[43] H.M. Cho, R. Tycko, A. Pines, J. Guckenheimer, Iterative maps for bistable excitation of two-level systems, Phys. Rev. Lett. 56 (1985) 1905–1908.
[44] R. Tycko, Iterative methods in the design of pulse sequences for NMR excitation, Adv. Magn. Reson, vol. 15, Academic Press, New York, 1990.
[45] J.J. Kotyk, J.R. Garbow, T. Gullion, Improvements in proton-detected NMR spectroscopy using spin-flip decoupling. An application to heteronuclear chemical shift correlation, J. Magn. Reson. 89 (1990) 647–653.
[46] M.J. Lizak, T. Gullion, M.S. Conradi, Measurement of like-spin dipole couplings, J. Magn. Reson. 91 (1991) 254–260.
[47] U. Haeberlen, J.S. Waugh, Coherent averaging effects in magnetic resonance, Phys. Rev. 175 (1968) 453–467.
[48] U. Haeberlen, High resolution NMR in solids: selective averaging, Adv. Magn. Reson. Suppl. 1 (1976).
[49] R.R. Ernst, G. Bodenhausen, A. Wokaun, Principles of Nuclear Magnetic Resonance In One and Two Dimensions, Clarendon Press, Oxford, 1987.
[50] J. Cavanagh, W.J. Fairbrother, A.G. Palmer III, N.J. Skelton, Protein NMR Spectroscopy, Academic Press, New York, 1996.
[51] S.J. Glaser, J.J. Quant, Homonuclear and heteronuclear Hartmann–Hahn transfer in isotropic liquids, Adv. Magn. Opt. Reson., vol. 19, Academic Press, San Diego, 1996, pp. 59–252.
[52] R.W. Dyksstra, A method to suppress cycling sidebands in broadband decoupling, J. Magn. Reson. 82 (1989) 347–351.
[53] E. Kupce, R. Freeman, G. Wider, K. Wüthrich, Suppression of cycling sidebands using bi-level adiabatic decoupling, J. Magn. Reson. A 122 (1996) 81–84.
[54] T.E. Skinner, M.R. Bendall, A phase-cycling algorithm for reducing sidebands in adiabatic decoupling, J. Magn. Reson. 124 (1997) 474–478.
[55] S. Zhang, D. Gorenstein, Adiabatic decoupling sidebands, J. Magn. Reson. 144 (2000) 316–321.
[56] Z. Zhou, R. Kümmerle, X. Qiu, D. Redwine, R. Cong, A. Taha, D. Baugh, B. Winniford, A new decoupling method for accurate quantification of polyethylene copolymer composition and triad sequence distribution with ^{13}C NMR, J. Magn. Reson. 187 (2007) 225–233.
[57] A.J. Shaka, P.B. Barker, R. Freeman, Three-spin effects in broadband decoupling, J. Magn. Reson. 71 (1987) 520–531.
[58] D. Suter, V. Schenker, A. Pines, Theory of broadband heteronuclear decoupling in multispin systems, J. Magn. Reson. 73 (1987) 90–98.
[59] J. Neves, B. Heitmann, N. Khaneja, S.J. Glaser, Heteronuclear decoupling by optimal tracking, J. Magn. Reson. 201 (2009) 7–17.
[60] N. Sunitha Bai, N. Hari, R. Ramachandran, J. Magn. Reson. A 106 (1994) 241.
[61] T. Hwang, M. Garwood, A. Tannus, P.C.M. van Zijl, J. Magn. Reson. A 121 (1996) 221.
[62] V. Sklenar, Z. Starcuk, Nuclear magnetic ^{13}C–^{19}F double resonance: fluorine broad band decoupling, Org. Magn. Reson. 22 (1984) 662.
[63] J.W.M. Jacobs, J.W.M. Van OS, W.S. Veeman, Broadband heteronuclear decoupling, J. Magn. Reson. 51 (1983) 56.
[64] Navin Khaneja, Problems in control of quantum systems, in: J. Gorman, B. Shapiro (Eds.), Control of MEMS to Atoms, Springer, US, in press.